Electronic Supplementary Material (ESI) for Journal of Materials Chemistry C.
This journal is © The Royal Society of Chemistry 2019

One-Dimensional π-π Stacking Induces Highly Efficient Pure Organic Room-Temperature Phosphorescence and Ternary-Emission Single-Molecule White Light

Yating Wen [a], Haichao Liu *[a], Shitong Zhang [a], Yu Gao [a], Yan Yan [b], and Bing Yang *[a]

[a] State Key Laboratory of Supramolecular Structure and Materials, College of Chemistry, Jilin University, Changchun 130012 (P.R. China). E-mail: hcliu@jlu.edu.cn; yangbing@jlu.edu.cn

[b] State Key Laboratory of Inorganic Synthesis and Preparative Chemistry, College of Chemistry, Jilin University, Changchun 130012 (P.R. China).

SI-1 The details of synthetic procedures

General information: All the reagents and solvents used for the synthesis were purchased from Aldrich and Acros companies and used without further purification. The synthesis procedure was presented in Scheme S1. ^{1}H and ^{13}C NMR spectra were recorded on a Bruker AVANCE 500 spectrometer at 500 MHz and 126 MHz, respectively, using tetramethylsilane (TMS) as the internal standard. The MALDI-TOF-MS mass spectra were recorded using an AXIMA-CFR^{TM} plus instrument.

TX and TX-Cl

TX and TX-Cl were purchased from Aldrich and Acros companies and purified by column chromatography on silica gel using dichloromethane/petroleum ether (1:3) as the eluent. TX: ^{1}H NMR (500 MHz, DMSO, 25 ℃, TMS): δ = 8.49 (dd, *J* = 8.1, 0.9 Hz, 2H), 7.87 (d, *J* = 7.6 Hz, 2H), 7.83 – 7.78 (m, 2H), 7.64 – 7.58 (m, 2H); ^{13}C NMR (126 MHz, $CDCl_3$, 25 ℃, TMS): δ = 137.276 (s, C), 132.246 (s, CH), 129.843 (s, CH), 129.243 (s, C), 126.286 (s, CH), 125.984 (s, CH); MALDI-TOF MS (mass *m/z*): 212.15 [M^+]. TX-Cl: ^{1}H NMR (500 MHz, DMSO, 25 ℃, TMS): δ = 8.49 (d, *J* = 8.0 Hz, 1H), 8.42 (d, *J* = 2.0 Hz, 1H), 7.97 (d, *J* = 8.6 Hz, 1H), 7.94 – 7.85 (m, 2H), 7.83 (t, *J* = 7.6 Hz, 1H), 7.64 (t, *J* = 7.6 Hz, 1H); ^{13}C NMR (126 MHz, $CDCl_3$, 25 ℃, TMS): δ = 178.594 (s, C), 136.786 (s, C), 135.352 (s, C), 132.455 (s, CH), 132.393 (s, CH), 130.086 (s, C), 129.830 (s, CH), 129.191 (s, CH), 128.612 (s, C), 127.346 (s, CH), 126.488 (s, CH), 125.965 (s, CH); MALDI-TOF MS (mass *m/z*): 246.19 [M^+].

The synthesis of 2-Bromothioxanthone (TX-Br)

The synthesis of 2-Bromothioxanthone (TX-Br) was referring to Ref. 1.[1]

α-mercaptobenzoic acid (5.4 g, 0.035 mol) was added portion-wise to concentrated sulfuric acid (50 ml, 98%) and excess bromobenzene (7.3 ml, 0.07 mol). The resulting suspension was stirred at room temperature for 24 hours, and then permitted to stand for an additional 1 hour on 100℃. The color rapidly changes from yellow to deep-red. The mixture was cooled and poured slowly over ice, filtered, and washed acid-free. Then extracted with chloroform, and the combined organic extracts were dried over anhydrous $MgSO_4$. After solvent removal, the crude product was further purified by column chromatography on silica gel using dichloromethane/petroleum ether (1:4) as the eluent. The product was isolated as a yellow solid (5.9 g, yield: 58%). ^{1}H NMR (500 MHz, DMSO, 25 °C, TMS): δ = 8.55 (d, *J*=2.2, 1H), 8.51 – 8.47 (m, 1H), 7.98 (dd, *J*=8.6, 2.3, 1H), 7.90 (t, *J*=7.5, 2H), 7.85 – 7.80 (m, 1H), 7.67 – 7.61 (m, 1H); ^{13}C NMR (126 MHz, $CDCl_3$, 25 °C, TMS): δ = 178.617 (s, C), 136.804 (s, C), 135.978 (s, C), 135.149 (s, CH), 132.542 (s, CH), 132.370 (s, CH), 130.387 (s, C), 129.928 (s, CH), 128.768 (s, C), 127.510 (s, CH), 126.567 (s, CH), 126.039 (s, CH), 120.228 (s, C); MALDI-TOF MS (mass *m/z*): 291.28 [M^+].

The synthesis of 2-Fluorothioxanthone (TX-F)

The synthetic procedure for TX-F is similar to that of TX-Br described above. A yellow solid were obtained in 51% yield. ^{1}H NMR (500 MHz, DMSO, 25 °C, TMS): δ = 8.48 (dd, *J* = 8.1, 1.0 Hz, 1H), 8.16 (dd, *J* = 9.7, 2.9 Hz, 1H), 7.99 (dd, *J* = 8.9, 5.0 Hz, 1H), 7.89 (d, *J* = 8.0 Hz, 1H), 7.84 – 7.78 (m, 1H), 7.75 (td, *J* = 8.8, 3.0 Hz, 1H), 7.65 – 7.59 (m, 1H); ^{13}C NMR (126 MHz, $CDCl_3$, 25 °C, TMS): δ = 179.02 (s, C), 161.14 (d, *J* = 247.5 Hz, C), 137.12 (s, C), 132.52 (s, C), 132.42 (s, CH), 130.75 (d, *J* = 6.1 Hz, C), 129.84 (s, CH), 128.22 (s, C), 127.94 (d, *J* = 7.1 Hz, CH), 126.44 (s, CH), 125.94 (s, CH), 120.96 (d, *J* = 24.1 Hz, CH), 115.27 (d, *J* = 22.9 Hz, CH). MALDI-TOF MS (mass *m/z*): 229.69 [M^+].

The synthesis of 2-Iodomothioxanthone (TX-I)

The synthetic procedure for TX-F is similar to that of TX-Br described above. A yellow solid were obtained in 56% yield. ^{1}H NMR (500 MHz, DMSO, 25 °C, TMS): δ = 8.73 (d, *J* = 1.8 Hz, 1H), 8.48 (d, *J* = 8.2 Hz, 1H), 8.09 (dd, *J* = 8.5, 1.9 Hz, 1H), 7.89 (d, *J* = 7.9 Hz, 1H), 7.82 (t, *J* = 7.6 Hz, 1H), 7.71 (d, *J* = 8.5 Hz, 1H), 7.62 (t, *J* = 7.1 Hz, 1H); ^{13}C NMR (126 MHz, $CDCl_3$, 25 °C, TMS): δ = 178.272 (s, C), 140.479 (s, CH), 138.424 (s, CH), 136.692 (s, C), 136.658 (s, C), 132.474 (s, CH), 130.325 (s, C), 129.857 (s, CH), 128.789 (s, C), 127.396 (s, CH), 126.494 (s, CH), 126.041 (s, CH), 90.844 (s, C); MALDI-TOF MS (mass *m/z*): 338.01 [M^+].

Synthetic routes to TX-Br, TX-F, TX-I

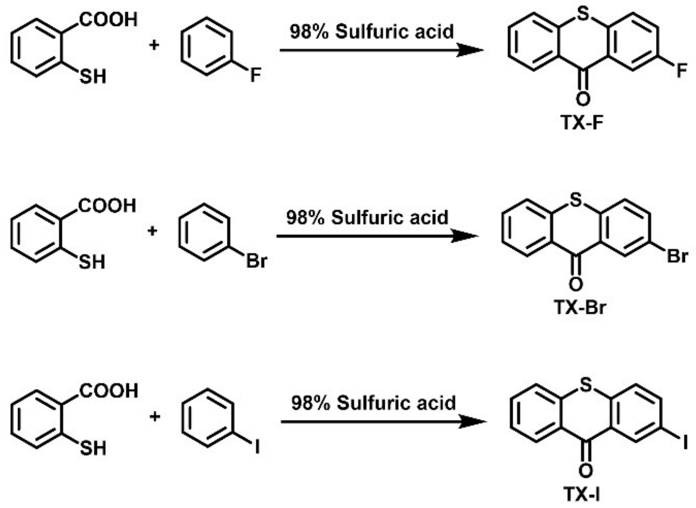

Scheme S1. Synthetic routes to TX-Br, TX-F and TX-I.

SI-2 Photophysical measurements: UV-vis spectra of solutions and films were recorded on a Shimadzu UV-3100 Spectrophotometer. Steady-state photoluminescence (PL) spectra and lifetimes were carried out with FLS980 Spectrometer. Quantum yield were measured using an integrating sphere apparatus. The solids were fixed on the quartz plate and placed in an integrating sphere apparatus for QY-measurement. The QY of thin films in vacuum were measured by slowly evaporating the solution in a closed quartz cell under vacuum condition until the film was formed and then placed in an integrating sphere apparatus. Solutions were placed in 1 cm path length quartz cells, and crystals were fixed on the quartz plate in terms of steady-state spectra and lifetimes.

The total lifetimes of multi-sectioned PL-decay spectra are calculated using the following equation:

$$\tau = \frac{\sum_{i=1}^{n} \tau_i^2 A_i}{\sum_{i=1}^{n} \tau_i A_i}$$

where τ is the lifetime, i represents for the number of the lifetime components, and A_i is the proportion for each lifetime components.

SI-3 Single crystal X-ray diffraction (XRD) data: Single crystals of TX, TX-Cl, TX-Br and TX-I were prepared by crystallization from the mixture of dichlomethane and methanol at room temperature. The diffraction experiments were carried out on a Rigaku R-AXIS RAPID diffractometer equipped with a Mo-Kα and control Software using the RAPID AUTO at 293 (±2) K. The crystal structures were solved with direct methods and refined with a full-matrix least-squares technique using the SHELXS programs. Powder XRD patterns were collected on a Rigaku SmartLab(3) diffractometer. Interplanar distance of molecular planars was measured based on the establishment of a plane on each TX moiety in the dimer using Mercury 3.9 Version software.

SI-4 Theoretical calculation: All the density functional theory (DFT) calculations were carried out using Gaussian 09 (version D.01) package on a Power Leader cluster.[2,3] The time-dependent density functional theory (TDDFT) and Tamm-Dancoff approximation (TDA-TDDFT) at the level of M06-2X/6-31G(d,p) were performed to optimize the geometries of monomer and dimer (representing the simplest aggregate) in the lowest singlet (S_1) and triplet (T_1) excited states, respectively, and natural transition orbitals (NTOs) were calculated to identify the excited-state property for both singlet and triplet states (Figure S16 and S17). The SOC coefficients were quantitatively estimated at the level of B3LYP/6-31G(d,p) by Beijing density function (BDF) program for monomer and dimer, respectively. [4-8]

SⅡ Figures and tables

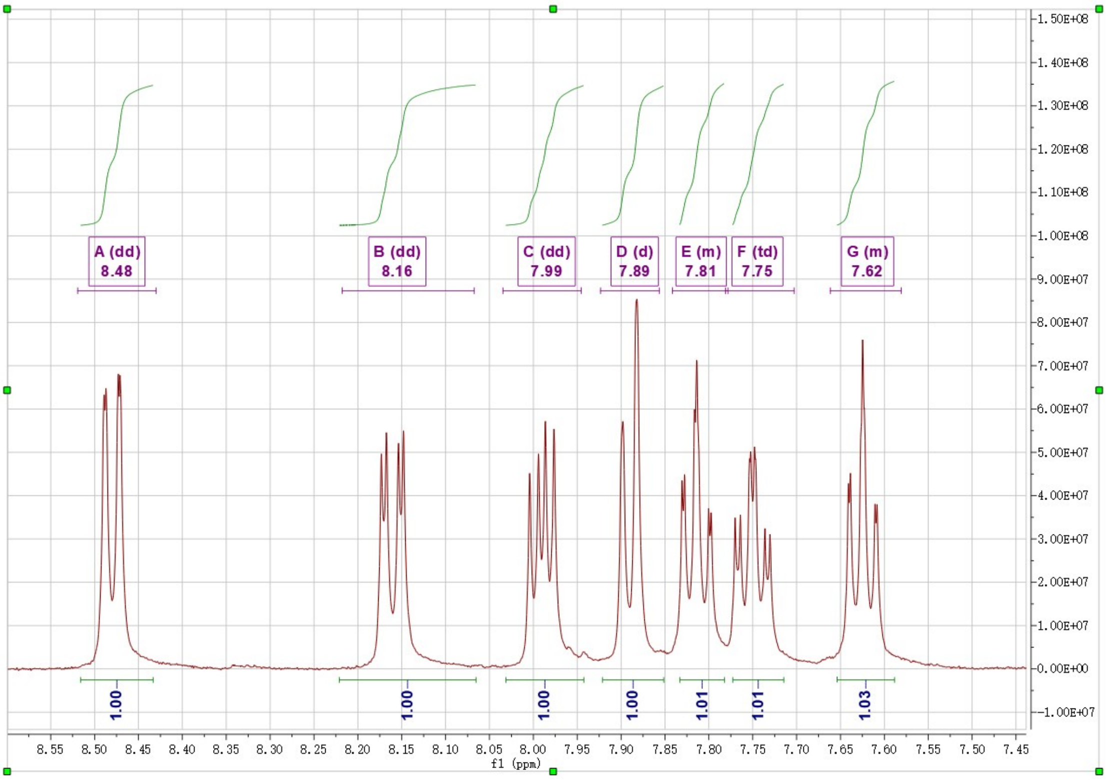

Figure S1. The ^{1}H NMR (500 MHz, DMSO, 25 ℃, TMS) of TX-F.

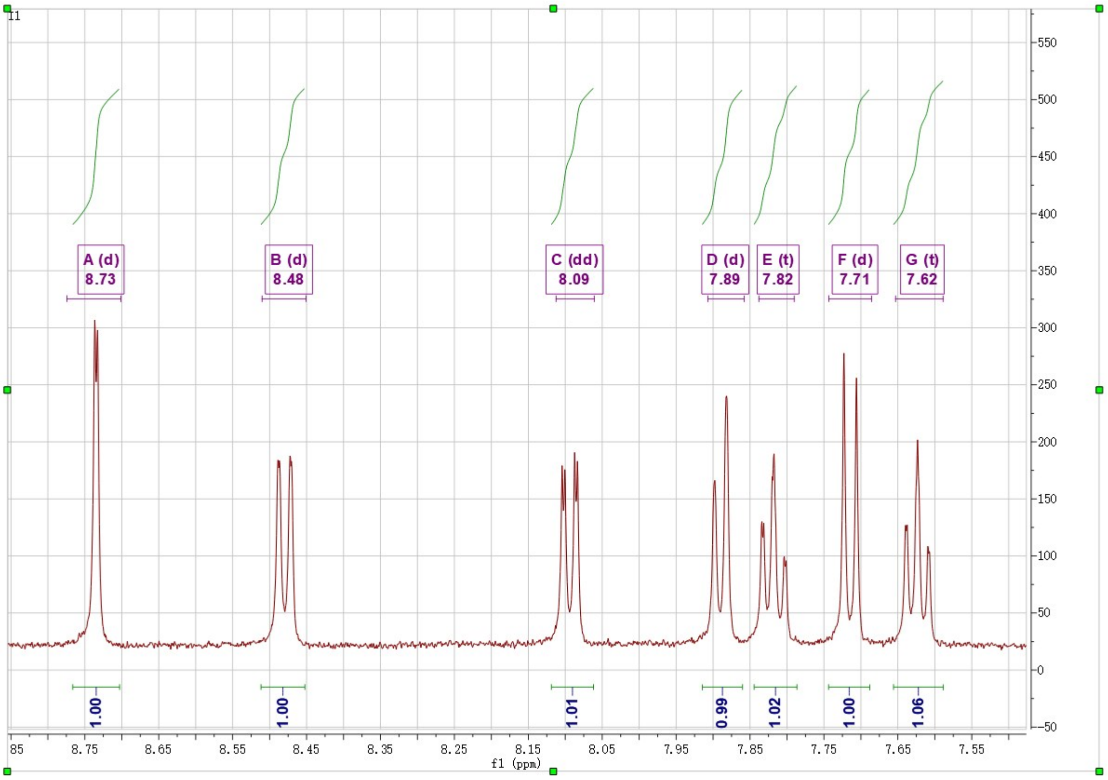

Figure S2. The ^{1}H NMR (500 MHz, DMSO, 25 ℃, TMS) of TX-I.

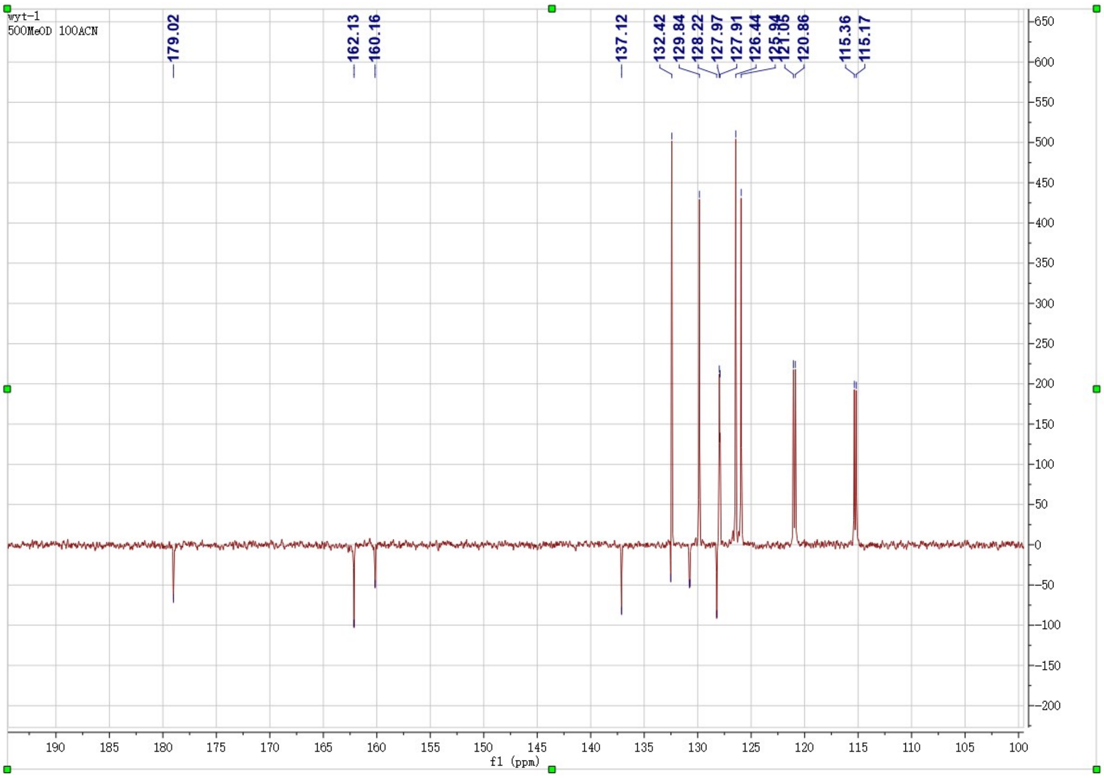

Figure S3. The ^{13}C NMR (126 MHz, $CDCl_3$, 25 ℃, TMS) of TX-F.

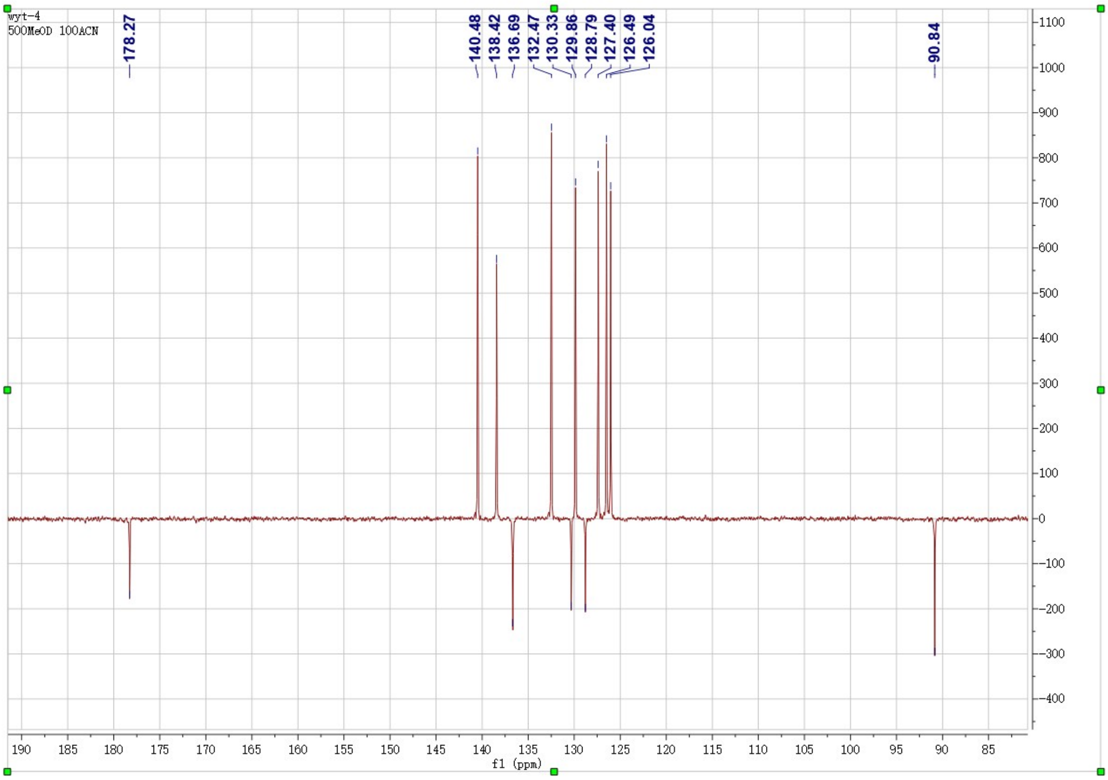

Figure S4. The ^{13}C NMR (126 MHz, $CDCl_3$, 25 ℃, TMS) of TX-I.

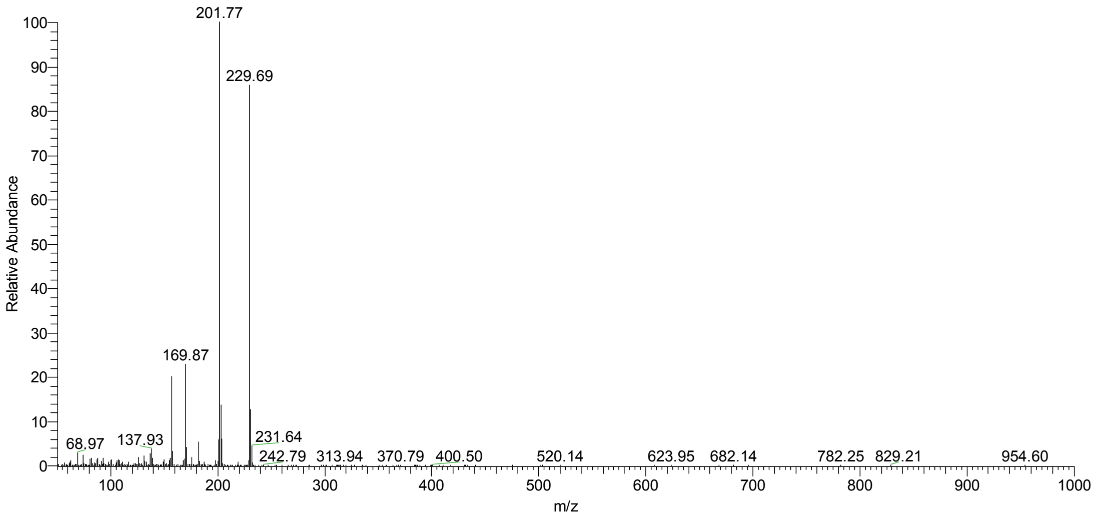

Figure S5. The MALDI-TOF MS spectrum of TX-F.

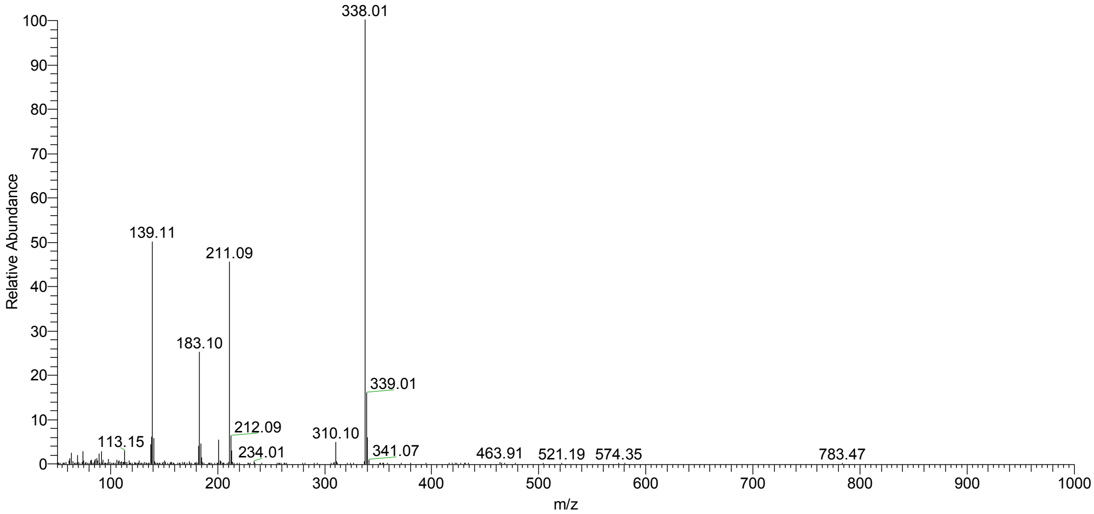

Figure S6. The MALDI-TOF MS spectrum of TX-I.

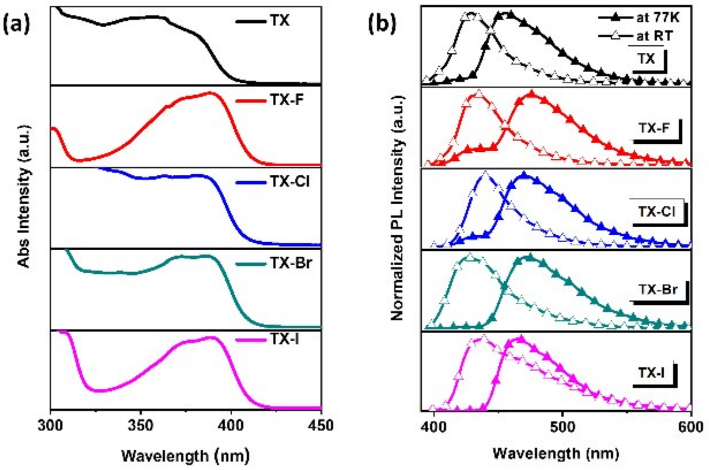

Figure S7. (a) Absorption and (b) emission spectra of all luminogens in monomer-molecule state (1 wt% doped film) at RT and 77 K.

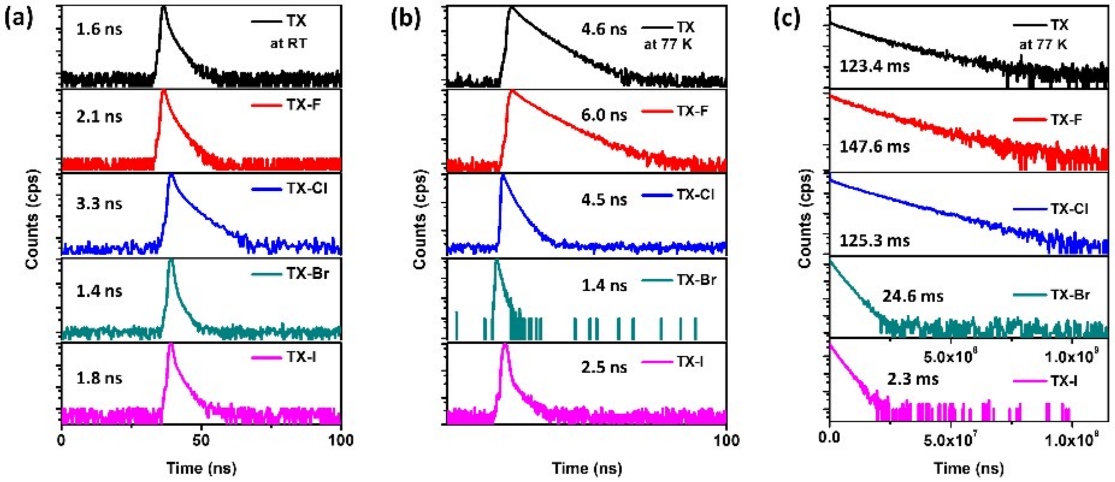

Figure S8. (a) Fluorescent lifetimes carried out at 430 nm of all luminogens in monomer-molecule state (1 wt% doped film) at RT. (b) Fluorescent lifetimes carried out at 430 nm of all luminogens in monomer-molecule state (1 wt% doped film) at 77 K. (c) Phosphorescent lifetimes carried out at 470 nm of all luminogens in monomer-molecule state (1 wt% doped film) at 77 K.

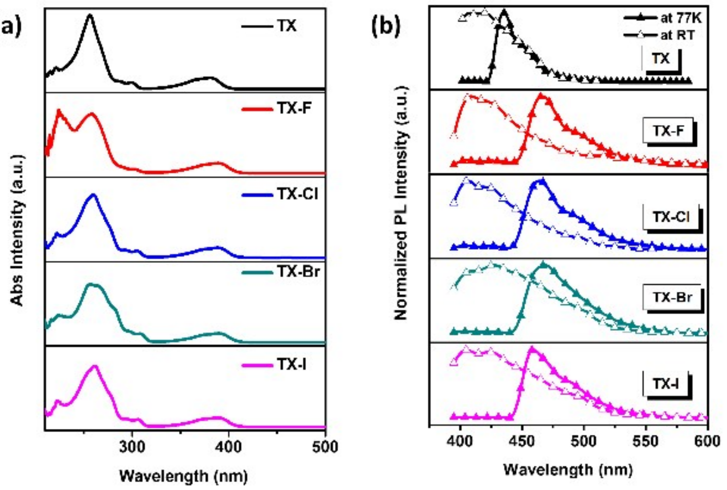

Figure S9. (a) Absorption and (b) emission spectra of all luminogens in monomer-molecule state (30 μM) in dichloromethane solutions at RT and at 77 K.

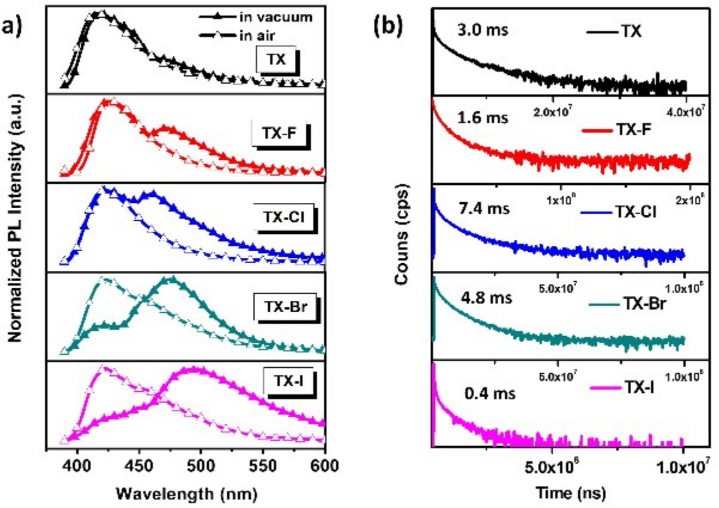

Figure S10. (a) Emission spectra of all luminogens in monomer-molecule state (1 wt% doped film) at RT and in vacuum. (b) Time-resolved spectra of all phosphorescent lifetimes carried out at 470 nm in monomer-molecule state (1 wt% doped film) at RT and in vacuum.

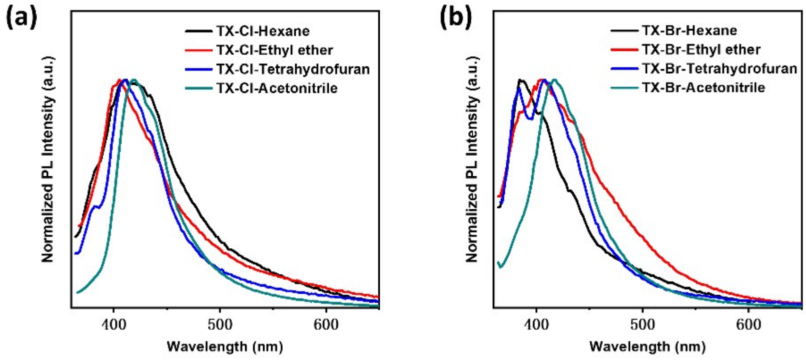

Figure S11. Emission spectra of (a) TX-Cl and (b) TX-Br in different polarity solvents (30 μM).

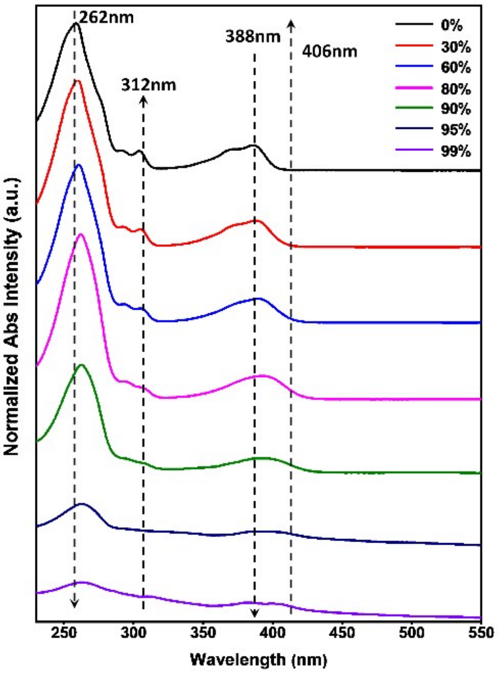

Figure S12. The absorption spectra of TX-Cl (30 μM) measured with increasing water content from 0 vol% to 99 vol % in THF/water mixtures.

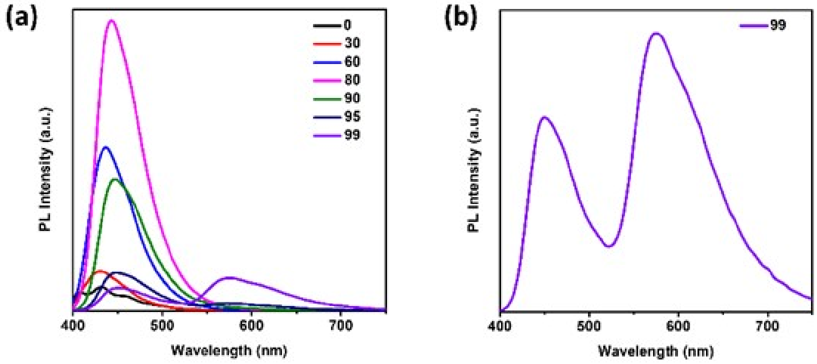

Figure S13. Emission spectra of TX-Cl (30 μM) in THF/water mixtures with increasing water content from 0 vol% to 99 vol %.

Compared with white emission of TX powder, both TX-Cl and TX-Br powders under UV irradiation exhibit bright orange phosphorescence-dominated emission at 578 nm together with an extremely weak emission in short wavelength, while both TX-F and TX-I powders show fluorescence-dominated blue emission in short wavelength. Relative to monomer phosphorescence at about 470 nm, it is very interesting that both TX-Cl and TX-Br powders display extraordinary bathochromic emission of 108 nm and significant enhancement in RTP intensity, respectively. Because both TX-Cl and TX-Br were excluded with strong charge-transfer (CT) excited state character (Figure S11), this long-wavelength emission can be ascribed to the aggregate RTP in powder. To further examine the aggregation effect, the emission spectra of TX-Cl in THF/water mixtures were recorded with increase of water fraction in volume ratio (Figure S13). When the water fraction is more than 95%, a new emission band around 578 nm begins to appear and then rises in intensity, implying the origin of aggregation.

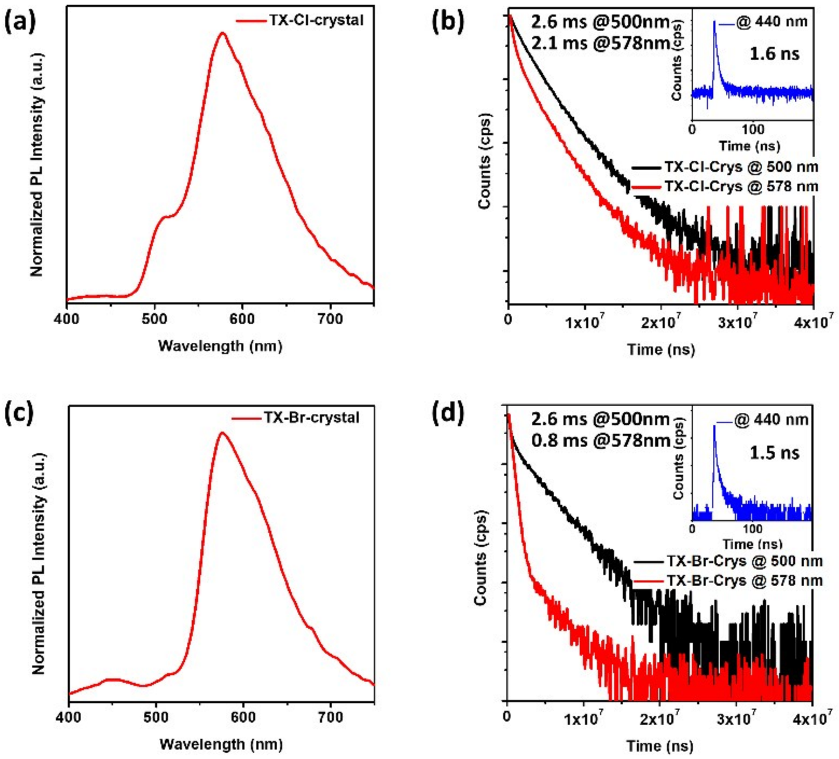

Figure S14. (a) Emission spectra and (b) lifetimes at different wavelength in TX-Cl crystal. (c) Emission spectra and (d) lifetimes at different wavelength in TX-Br crystal.

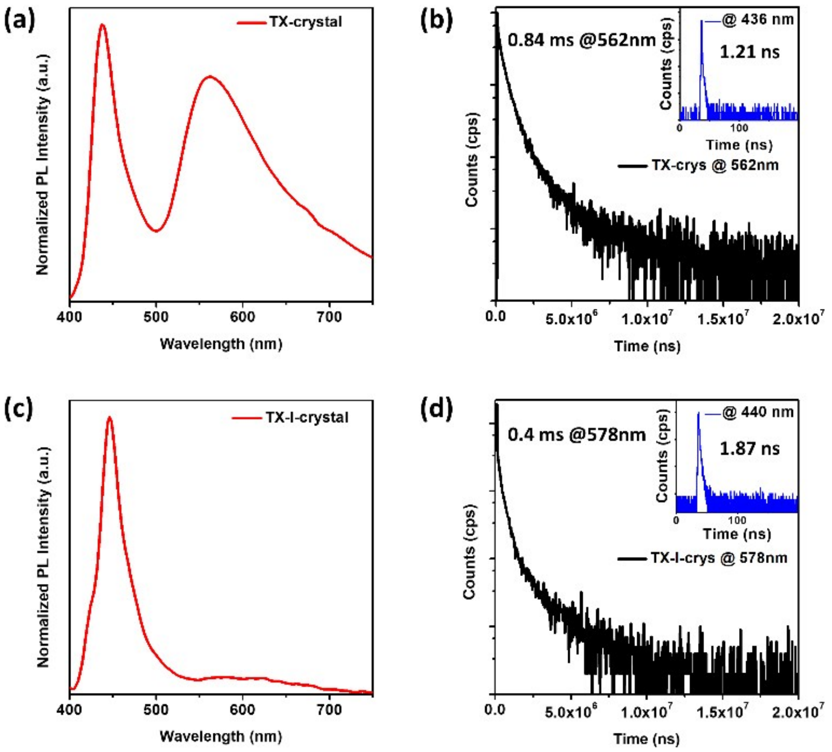

Figure S15. (a) Emission spectra and (b) lifetimes at different wavelength in TX crystal. (c) Emission spectra and (d) lifetimes at different wavelength in TX-I crystal.

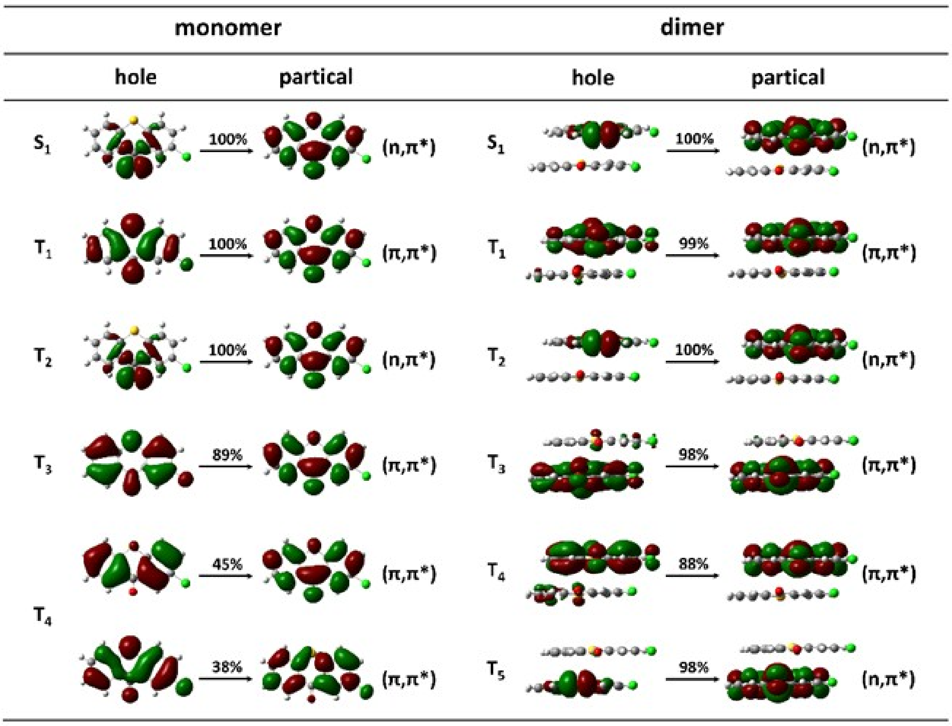

Figure S16. NTOs of the monomer and dimer in the lowest single state (S_1) and triplet manifolds (T_n) based on the geometry of S_1 state.

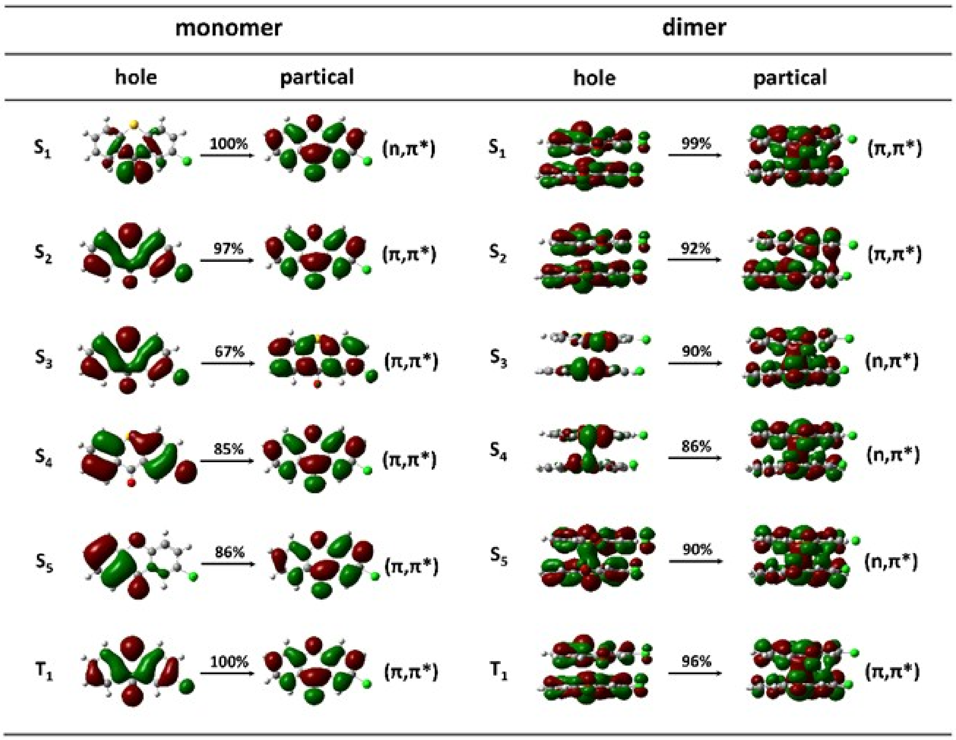

Figure S17. NTOs of the monomer and dimer in the single manifolds (S_n) and the lowest triplet state (T_1) based on the geometry of T_1 state.

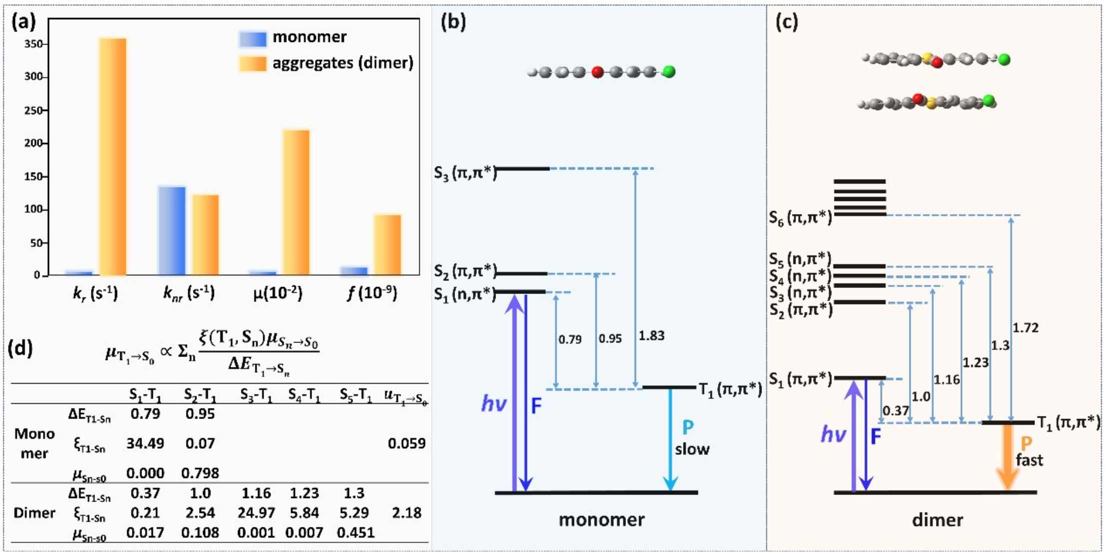

$$\mu_{T_1 \to S_0} \propto \Sigma_n \frac{\xi(T_1, S_n)\mu_{S_n \to S_0}}{\Delta E_{T_1 \to S_n}}$$

		S_1-T_1	S_2-T_1	S_3-T_1	S_4-T_1	S_5-T_1	$u_{T_1 \to S_0}$
Mono mer	$\Delta E_{T1\text{-}Sn}$	0.79	0.95				
	$\xi_{T1\text{-}Sn}$	34.49	0.07				0.059
	$\mu_{Sn\text{-}s0}$	0.000	0.798				
Dimer	$\Delta E_{T1\text{-}Sn}$	0.37	1.0	1.16	1.23	1.3	
	$\xi_{T1\text{-}Sn}$	0.21	2.54	24.97	5.84	5.29	2.18
	$\mu_{Sn\text{-}s0}$	0.017	0.108	0.001	0.007	0.451	

Figure S18. (a) k_r and k_{nr} were obtained based on the experimental determination of monomer and aggregate state of TX-Cl; the comparison of transition dipole moment μ (rough estimation) and oscillator strength f of $T_1 \rightarrow S_0$ is from theoretical calculations between monomer and dimer of TX-Cl. (b) The comparison of SOC calculation and energy level diagram between monomer and (c) dimer of TX-Cl for the understanding of high-efficiency RTP emission in one-dimensional π-π aggregates. (d) The rough estimation process of $\mu_{T1 \rightarrow} S_0$ for both monomer and dimer.

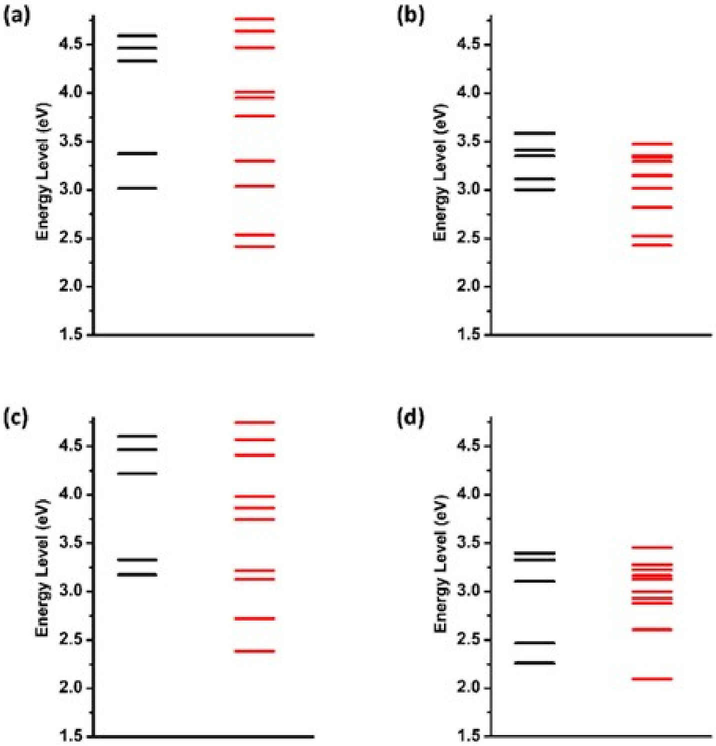

Figure S19. (a) The energy level diagram of monomer and (b) dimer based on the geometry of S_1 state. (c)The energy level diagram of monomer and (d) dimer based on the geometry of T_1 state.

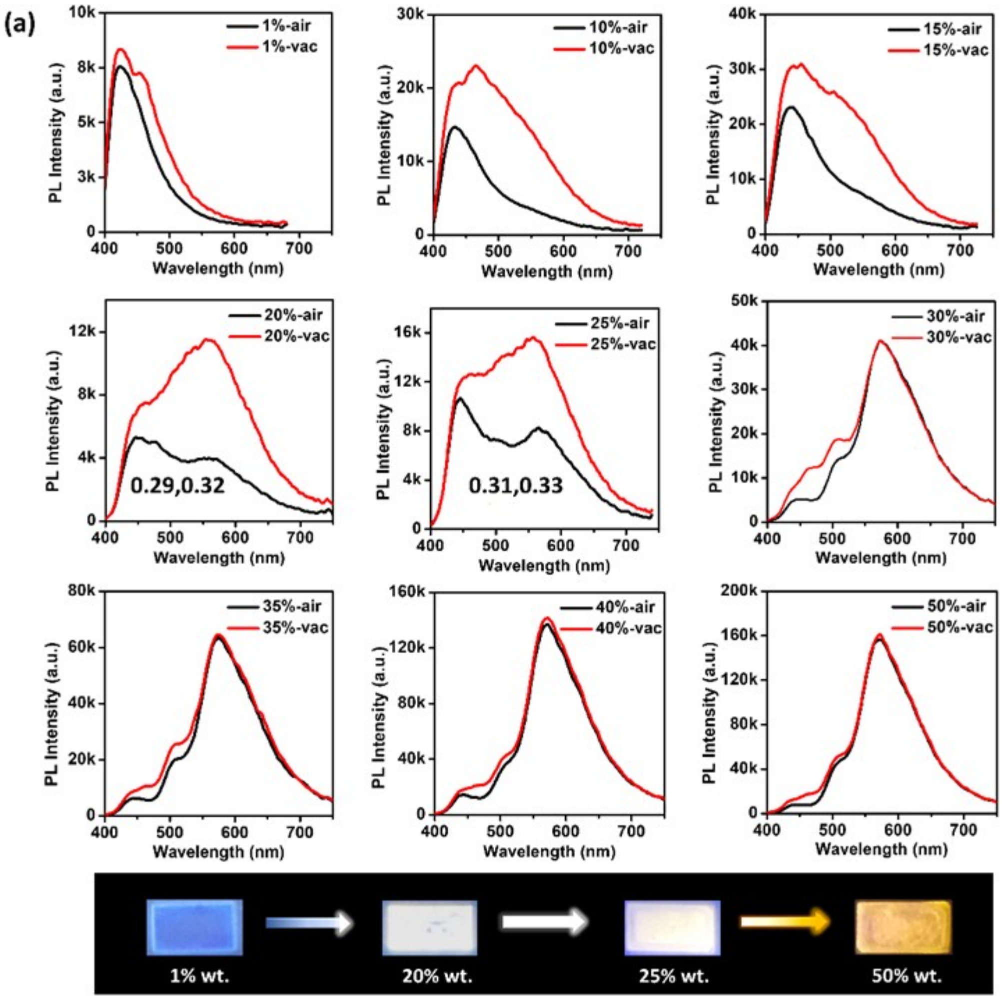

Figure S20. Emission spectra of TX-Cl in air and in vacuum with increasing doping ratio in PMMA films.

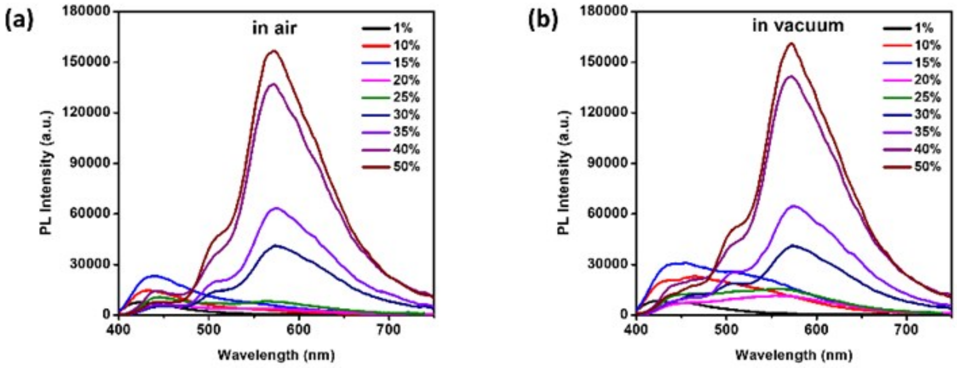

Figure S21. (a) The variation tendency of emission spectra of TX-Cl in air with increasing doping ratio in PMMA films. (b) The variation tendency of emission spectra of TX-Cl in vacuum with increasing doping ratio in PMMA films.

For the doping ratio less than 15 wt%, the emission is dominated by blue fluorescence. Once deoxygenation, the obvious emission enhancement is observed in long-wavelength band, indicating the typical oxygen-sensitive phosphorescence. With continuous increase of doping ratio, RTP emissions become so strong that they are comparable with the fluorescence in intensity. In particular, the films with the doping ratio of 20%wt. and 25%wt. exhibit very excellent SMWLE with the CIE coordinates of (0.29, 0.32) and (0.31, 0.33) respectively, as a result of the coexisting ternary emissions: monomer fluorescence (blue), monomer RTP (green) and aggregate RTP (orange), corresponding to a right ratio of aggregate to monomer in doped film. More importantly, the SMWLE can be finely modulated from cool to warm white light by precisely controlling the aggregate degree through the tuning of the doping ratio of TX-Cl in PMMA film (**Figure 4** and S20). When the doping ratio is more than 50%wt., the emission spectrum profiles almost keep the same as those of crystal and powder, indicating the aggregate formation with the similar molecular packing in crystal and powder. The powder XRD experiment also confirmed the same diffraction patterns between powder and 50%wt. doped film (Figure S22), corresponding to the same microcrystalline structure in aggregates. At this time, this kind of aggregate shows the almost invariable RTP emission intensity in the presence or absence of oxygen, which means the invalidation of oxygen-quenching as a result of very good impermeability of oxygen in aggregates. This point is very important for the practical applications of pure organic RTP materials under ambient conditions.

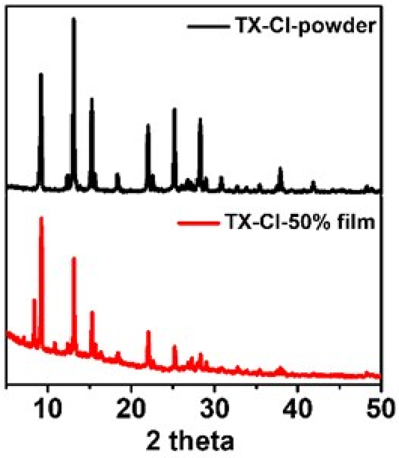

Figure S22. XRD patterns in aggregation of powder and 50%wt. doped film of TX-Cl in PMMA.

Table S1. Photophysical properties of the luminogens in monomer-molecule state (doped film).

	TX	TX-F	TX-Cl	TX-Br	TX-I
λ_{abs} [nm]	384	392	391	392	392
λ_{emRT} [nm]	429	433	436	428	436
λ_{em77K} [nm]	429/456	433/473	436/470	428/470	436/467
λ_{emRT} in vacuum[nm]	420/463	430/471	430/470	425/473	433/473
$\tau_{F\ RT}$[ns]	1.6	2.1	3.3	1.4	1.8
$\tau_{F\ 77K}$[ns]	4.6	6.0	4.5	1.4	2.5
$\tau_{P\ 77K}$[ms]	123.4	147.6	125.3	24.6	2.3
$\tau_{P\ RT}$ in vacuum[ms]	3.0 τ_1=0.18ms (22.46%) τ_2=1.04ms (50.39%) τ_3=4.07ms (27.15%)	11.6 τ_1=0.98ms (28.30%) τ_2=4.48ms (50.68%) τ_3=16.9ms (21.02%)	7.4 τ_1=0.62ms (23.30%) τ_2=2.84ms (50.99%) τ_3=10.3ms (25.72%)	4.8 τ_1=0.51ms (20.55%) τ_2=2.22ms (51.22%) τ_3=6.69ms (28.23%)	0.4 τ_1=18.7μs (64.63%) τ_2=116μs (22.85%) τ_3=504μs (12.52%)

λ_{abs} = absorption peak; λ_{em} = emission peak; τ_F = fluorescent lifetime; τ_P = phosphorescent lifetime.

Table S2. Photophysical properties of the luminogens in powder.

TX		TX-F		TX-Cl		TX-Br		TX-I	
λ_{em} [nm]	τ	λ_{em} [nm]	τ	λ_{em} [nm]	τ	λ_{em} [nm]	τ	λ_{em} [nm]	τ
430	1.5ns τ_1=0.53ns (91.77%) τ_2=3.33ns (8.23%)	450	1.37ns	440	1.82ns τ_1=1.12ns (95.16%) τ_2=4.97ns (4.84%)	440	1.43ns τ_1=0.79ns (97.24%) τ_2=4.98ns (2.76%)	445	1.48ns τ_1=0.49ns (95.02%) τ_2=3.88ns (4.98%)
				500	1.5ms τ_1=0.38ms (32.5%) τ_2=1.63ms (67.5%)				
560	0.83ms τ_1=0.18ms (29.78%) τ_2=0.89ms (70.22%)	530	1.34ms τ_1=0.23ms (59.9%) τ_2=1.58ms (40.1%)	578	1.33ms τ_1=0.52ms (58.48%) τ_2=1.68ms (41.52%)	578	0.83ms τ_1=0.34ms (70.53%) τ_2=0.76ms (26.64%) τ_3=2.63ms (2.83%)	578	0.36ms τ_1=0.02ms (68.1%) τ_2=0.4ms (32.9%)

Table S3. Photophysical properties of the luminogens in crystal.

TX		TX-Cl		TX-Br		TX-I	
λ_{em} [nm]	τ	λ_{em} [nm]	τ	λ_{em} [nm]	τ	λ_{em} [nm]	τ
435	1.21ns τ_1=0.53ns (96.14%) τ_2=3.66ns (3.86%)	440	1.6ns τ_1=0.92ns (60.25%) τ_2=2.01ns (39.75%)	440	1.5ns τ_1=0.82ns (67.25%) τ_2=2.01ns (32.75%)	440	1.87ns τ_1=0.78ns (71.38%) τ_2=2.66ns (28.62%)
		500	2.6ms τ_1=0.63ms (7.98%) τ_2=2.02ms (76.34%) τ_3=4.19ms (15.68%)	500	2.6ms τ_1=0.32ms (20.24%) τ_2=2.66ms (79.76%)		
560	0.84ms τ_1=9.49μs (16.02%) τ_2=0.30ms (56.64%) τ_3=1.12ms (29.34%)	578	2.1ms τ_1=0.3ms (26.47%) τ_2=1.3ms (32.76%) τ_3=2.57ms (40.77%)	578	0.8ms τ_1=0.31ms (68.8%) τ_2=0.44ms (28.46) τ_3=2.68ms (2.74%)	578	0.4ms τ_1=0.06ms (64.2%) τ_2=0.48ms (35.8%)

Table S4. Photophysical parameters of monomer state in doped film at room temperature.

Compound	$\langle\tau\rangle_F$	Φ_F	k_r^F	k_{nr}^F	$\langle\tau\rangle_P$[	Φ_P	k_r^P	k_{nr}^P	k_{ISC}
	[ns]	[%]	[s^{-1}]	[s^{-1}]	ms]	[%]	[s^{-1}]	[s^{-1}]	[s^{-1}]
TX	1.6	1.04	6.5×10^6	6.2×10^8	3.0	0.46	1.53	3.32×10^2	2.8×10^6
TX-F	2.1	1.5	7.1×10^6	4.6×10^8	11.6	1.2	1.04	0.85×10^2	5.7×10^6
TX-Cl	3.3	0.55	1.7×10^6	3.0×10^8	7.4	0.95	1.28	1.34×10^2	2.9×10^6
TX-Br	1.4	0.2	1.4×10^6	7.0×10^8	4.8	1.7	3.54	2.05×10^2	12.1×10^6
TX-I	1.8	0.04	0.2×10^6	5.5×10^8	0.36	0.46	12.7	27.6×10^2	2.6×10^6

$k_r^P = \Phi_P / \langle\tau\rangle_P$, $k_{nr}^P = (1- \Phi_P) / \langle\tau\rangle_P$, $k_r^F = \Phi_F / \langle\tau\rangle_F$, $k_{nr}^F = (1- \Phi_F- \Phi_P) / \langle\tau\rangle_F$, $k_{ISC} = \Phi_P / \langle\tau\rangle_F$.

The Φ_P is measured under deoxygenation condition.

Table S5. Photophysical parameters of aggregate state in crystals at room temperature.

Compound	$\langle\tau\rangle_F$	Φ_F	k_r^F	k_{nr}^F	$\langle\tau\rangle_P$	Φ_P	k_r^P	k_{nr}^P	k_{ISC}
	[ns]	[%]	[s^{-1}]	[s^{-1}]	[ms]	[%]	[s^{-1}]	[s^{-1}]	[s^{-1}]
TX	1.21	0.6	5.0×10^6	8.1×10^8	0.84	0.9	10.8	11.8×10^2	7.4×10^6
TX-F	1.37	0.7	5.1×10^6	7.2×10^8	1.34	0.7	5.2	7.4×10^2	5.1×10^6
TX-Cl	1.6	0.3	1.9×10^6	1.6×10^8	2.1	74.7	3.6×10^2	1.2×10^2	4.7×10^8
TX-Br	1.5	0.4	2.7×10^6	5.5×10^8	0.8	17.6	2.2×10^2	10.3×10^2	1.2×10^8
TX-I	1.87	0.4	2.1×10^6	5.3×10^8	0.4	0.1	2.5	25×10^2	0.5×10^6

$k_r^P = \Phi_P / \langle\tau\rangle_P$, $k_{nr}^P = (1- \Phi_P) / \langle\tau\rangle_P$, $k_r^F = \Phi_F / \langle\tau\rangle_F$, $k_{nr}^F = (1- \Phi_F- \Phi_P) / \langle\tau\rangle_F$, $k_{ISC} = \Phi_P / \langle\tau\rangle_F$

Table S6. The SOC coefficients between excited singlet and triplet states based on S_1 state geometry of TX-Cl monomer and dimer. The unit of SOC coefficient is cm^{-1}.

	S_0-T_1	S_1-T_1	S_1-T_2	S_1-T_3	S_1-T_4	S_1-T_5	S_1-T_6	S_1-T_7	S_1-T_8	S_1-T_9	S_1-T_{10}
monomer	0.20	38.10	0.01	14.53	0.79	1.25	7.53	11.02	0.96	11.22	2.45
dimer	4.76	36.66	4.02	0.78	15.90	0.30	0.98	1.19	0.88	0.19	1.18

Table S7. The SOC coefficients between excited singlet and triplet states based on T_1 state geometry of TX-Cl monomer and dimer. The unit of SOC coefficient is cm^{-1}.

	S_0-T_1	S_1-T_1	S_2-T_1	S_3-T_1	S_4-T_1	S_5-T_1
monomer	0.12	34.49	0.07	1.06	0.36	0.15
dimer	4.60	0.21	2.54	24.97	5.84	5.29

Table S8. Crystallographic data.

	TX	TX- Cl	TX-Br	TX-I
crystal color	colorless	yellow	yellowish	colorless
empirical formula	$C_{13}H_8OS$	$C_{13}H_7ClOS$	$C_{13}H_0BrOS$	$C_{13}H_7IOS$
formula weight	212.25	246.70	284.10	338.16
T [K]	100(2)	299(2)	293(2)	289(2)
crystal system	monoclinic	triclinic	triclinic	orthorhombic
space group	P 1 21/c 1	P -1	P -1	P 21 21 21
a [Å]	15.6308(10)	3.8774(3)	3.9237(10)	4.1712(3)
b [Å]	3.9100(2)	7.2116(6)	7.2727(19)	6.4807(4)
c [Å]	15.6582(10)	19.1149(14)	19.173(5)	43.775(3)
α [°]	90	88.416(6)	88.393(4)	90
β [°]	100.879(2)	88.918(6)	88.616(4)	90
γ [°]	90	82.032(6)	82.487(4)	90
V [Å^3]	939.77(10)	529.07(7)	542.1(2)	1128.57(13)
Z	4	2	2	1
F(000)	440	252	274	940
density [g/cm^3]	1.500	1.549	1.741	2.623
μ [mm^{-1}]	0.306	4.796	3.953	5.476
reflections collected	29944	8357	3390	17654
unique reflections	3338	1290	2186	1642
R (int)	0.0331	0.1031	0.0319	0.1522
GOF	1.093	0.876	1.023	1.043
R_1 [I>2σ(I)]	0.0573	0.0518	0.0654	0.0599
$ωR_2$ [I>2σ(I)]	0.1528	0.1203	0.1792	0.1506
R_1 (all data)	0.0782	0.1033	0.0837	0.0647
$ωR_2$ (all data)	0.1689	0.1466	0.1913	0.1540
CCDC	1911710	1911704	1911705	1911709

SⅢ References

1 H. GILMAN and J. W. DIEHL, J. Org. Chem., 1959, 24, 1914-1916.

2 R. A. Gaussian09, Inc., Wallingford CT, 2009, 121, 150-166.

3 R. L. Martin, J. Chem. Phys., 2003, 118, 4775-4777.

4 W. Liu, F. Wang and L. Li, J. Theor. Comput. Chem., 2003, 2, 257-272.

5 Z. Li, B. Suo, Y. Zhang, Y. Xiao and W. Liu, Mol. Phys., 2013, 111, 3741-3755.

6 Z. Li, Y. Xiao and W. Liu, J. Chem. Phys., 2012, 137, 154114.

7 Z. Li, Y. Xiao and W. Liu, J. Chem. Phys., 2014, 141, 054111.

8 M. Quaranta, S. M. Borisov and I. Klimant, Bioanal. Rev., 2012, 4, 115-157.